# Characterization of a 600 A Barium Oxide-Based Hollow Cathode

## IEPC-2025-706

Presented at the 39th International Electric Propulsion Conference, Imperial College London, London,
United Kingdom
14-19 September 2025

Roberto Martelli\*, John D. Williams<sup>†</sup>, Seth Thompson<sup>‡</sup>, and Tait Freestone<sup>§</sup> Colorado State University, Fort Collins, CO, 80523, U.S.A.

Casey Farnell  $\P$  Plasma Controls, LLC. Fort Collins, CO, 80523, U.S.A.

As power levels rise in Hall thruster (HT)-based electric propulsion devices, so do the current requirements on their cathodes. Such cathodes also have lifetime requirements in the many kilohour range at these high currents for sustained thrust maneuvers. Traditional hollow cathodes typically use inserts as the electron emitter that are made from monolithic LaB<sub>6</sub> or porous tungsten that is impregnated with a BaO containing ceramic material-specifically barium calcium aluminate. A hollow cathode capable of supplying 500A over such lifetimes has been developed and tested using a LaB<sub>6</sub> insert, but one using a BaO insert at these currents has not, except for some preliminary testing in MPDs. This paper presents the design and characterization of a cathode operating at sustained discharge currents up to 600A using a tungsten and barium-calcium-alumina-scandate (BCA-S) cermet insert. The insert, formed in a one-step firing process from tungsten, BaCO<sub>3</sub>, CaCO<sub>3</sub>, Al<sub>2</sub>O<sub>3</sub>, and Sc<sub>2</sub>O<sub>3</sub> powders offers lower production costs, in addition to lower operating temperatures due to the lower work function of BaO-based emitters. Operation data is presented on Argon and Krypton as propellants at a range of currents and flow rates with discussion of stable versus unstable operating modes, and a preliminary estimate of the cathode's operational lifetime.

<sup>¶</sup>President, Plasma Controls, LLC., Casey.Farnell@colostate.edu



<sup>\*</sup>PhD Student, Department of Mechanical Engineering, roberto.martelli@colostate.edu.

<sup>&</sup>lt;sup>†</sup>Professor, Department of Mechanical Engineering, john.d.williams@colostate.edu.

<sup>&</sup>lt;sup>‡</sup>Research Scientist, Department of Mechanical Engineering, seth.thompson@colostate.edu.

<sup>§</sup>Research Scientist, Department of Mechanical Engineering, tait.freestone@colostate.edu.

# I. Introduction

Cathodes are an integral component to electric propulsion devices; from gridded-ion thrusters (GITs) to Hall thrusters (HETs) to magnetoplasmadynamic thrusters (MPDs), a source of free electrons is critical to continued operation. GITs and HTs in particular have used hollow cathodes to provide ionization and plume-neutralization electron currents for decades. The defining feature of a cathode's performance and lifetime tends to be its electron-emitting insert material, which is engineered to maintain a low work function and high emission current density throughout the life of the thruster - up to the range of hundreds of kilohours for sustained-thrust maneuvers. When thruster requirements have called for high electron currents (>50A), as they have been doing with increasing frequency, the insert material of choice has been Lanthanum Hexaboride (LaB<sub>6</sub>) due to its high emission current density and low evaporation rate when compared to the alternative used at lower currents - barium-calcium-aluminate (BCA) dispensers [1, 2]. Where LaB<sub>6</sub> inserts are a monolithic insert material, BCA dispenser style inserts are instead a composite, with a porous tungsten matrix infiltrated with the BCA material. The barium oxide within the BCA ceramic is released via thermal decomposition at elevated temperatures as a vapor, which adheres to the tungsten and forms a surface with a work function around 2eV, or as low as 1.6eV if scandate is included in the ceramic [3]. This is in contrast to the 2.6-2.9eV work function range for LaB<sub>6</sub>, which means an increase in operation temperatures of about 500°C, from ~1100°C to ~1600°C at 10A/cm<sup>2</sup> emission currents. This operation temperature, in the absence of contaminants in the propellant, is the primary determining factor in the cathode lifetime, as the bulk LaB<sub>6</sub>, or Ba/BaO within the ceramic impregnant evaporates and is lost. In the case of BCA dispenser cathodes, the evaporation rate of Ba/BaO can exceed its diffusion rate through the tungsten pores, leading to a reduction in internal Ba/BaO vapor pressures and loss of coverage of the tungsten [2]. Loss of this coverage means an increase in the insert work function and subsequent severe worsening of insert performance. For this reason, BCA dispenser cathodes are primarily used in applications where their emission current densities - and thus operation temperatures - remain low. The degradation of a BCA insert has been shown in a study with BCA hollow cathodes at extreme current densities in an MPD within 10 hours of operation [4], however the current densities tested were in the hundreds of amps per cm<sup>2</sup>, which is substantially beyond current requirements for HTs or GITs.

Plasma Controls, a company closely associated with CSU's Electric Propulsion and Plasma Engineering Lab (CEPPE Lab), has developed a variation of the BCA cathode, where the insert is formed in a single-step process, as opposed to first forming porous tungsten, then infiltrating it with ceramic [5]. Such inserts have shown to operate far above  $20A/cm^2$  without noted degradation in performance, in contrast to typical cathodes of similar composition. This performance, alongside the ease of manufacture of the inserts, makes the material a promising candidate for high-current cathode inserts. Should this prove successful, it would represent an alternative to LaB<sub>6</sub> in high current hollow cathodes, where the lower operation temperatures would reduce the design challenges associated with heating the insert at startup and controlling the heat generated by the cathode during operation, which have been present in high-current LaB<sub>6</sub> cathodes [1]. This paper further aims to identify new challenges with high current BCA inserts, and the steps necessary in design or future testing to address them.

# II. Test Setup

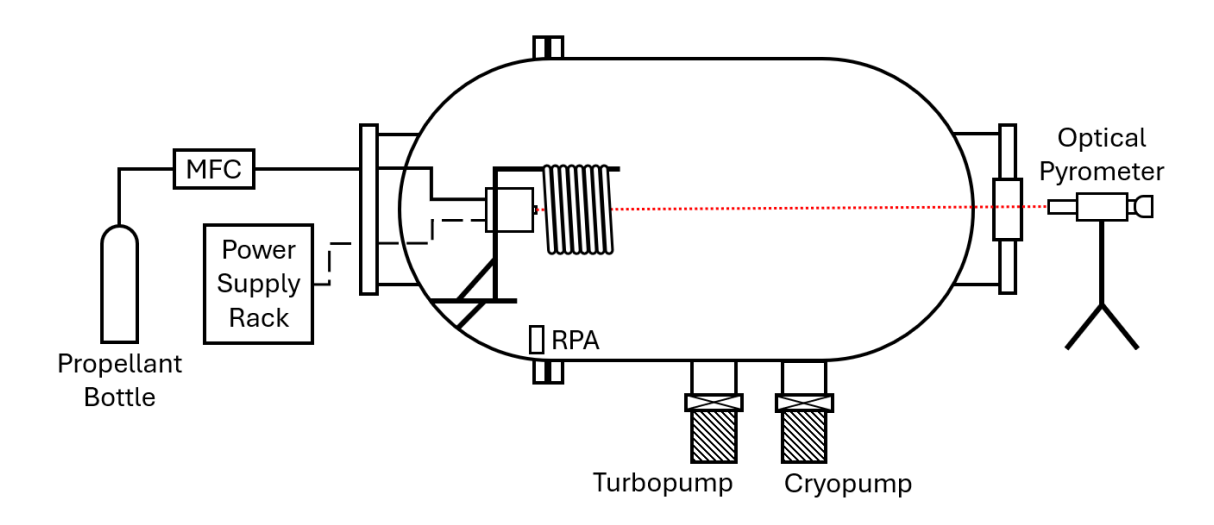
## A. Facility and Testing Apparatus

The 600A cathode was tested in CEPPE Lab's Cygnus Vacuum Test Facility, a 1.2m diameter by 4.6m long vacuum chamber pumped to vacuum by both a cryopump and turbopump mounted to flanges on the chamber floor, as seen in figure 1. This pumping scheme achieves pressures of  $1\mu$ Torr (133  $\mu$ Pa) with no gas flow. The maximum pressure observed was 3mTorr (0.4Pa) at the mass flow controller's maximum flow of 1000 standard cubic centimeters per minute (sccm) of Krypton through the cathode. Propellant gasses of Argon and Krypton are supplied by compressed gas bottles, fed through a pressure regulator to reduce pressures upstream of the MFC to 100psi (690kPa). The mass flow controller is controlled digitally, and is



consistently within 1% of the target flow rate. Power is supplied to the cathode components and magnetic coils from a rack of power supplies through isolated electrical feedthroughs. The electrical setup is detailed further later in this section. The anode is made from copper tubing coiled with an internal diameter of 12 inches (30.5cm). Water is flowed through the anode coil during operation to prevent damage to the copper from excessive heating and minimize thermal facility effects.

A retarding potential analyzer (RPA) is mounted to the chamber floor, located axially between the keeper orifice plate and the upstream face of the anode and radially at 0.5 meters from the cathode's centerline. The RPA has four biased grids to reject electrons selectively reject ions of increasing energy from a grounded collector plate, which records the ion current. Recording the change in current as the ion rejection voltage is increased provides a distribution function for the ion energies within the plasma. At the far end of the chamber, an optical pyrometer is directed through a window in the vacuum chamber to the cathode's orifice plate. The optical pyrometer uses a 'disappearing' filament which is resistively heated to match the emission of the measured surface, then the filament's known temperature profile is used to determine the surface temperature.



 $Figure \ 1. \ Cygnus \ Testing \ Facility \ Diagram$ 

To replicate the cathode's operation within a thruster, a magnetic field simulator as described in [6] is used to generate a strong magnetic field (400-600 Gauss) at the downstream end of the cathode, shown in figure 2 as the 'High Field Region'. The simulator consists of a large copper wire coil in a 1018 steel housing, designed in magnetic modeling software to match a typical hall thruster field profile. Although a considerably smaller simulator could have been made using specialized magnetic materials such as pure iron or Hiperco, the present material was found to have acceptable performance with a significant reduction in cost. The magnetic coil body is isolated from the chamber ground. Shown in figure 2 is the cathode gas feed tube, which uses a ceramic isolator along the flow path to prevent coupling to ground. A total of 3 thermocouples are placed at the upstream end, midpoint, and downstream end of the magnetic coils. These thermocouples are used to ensure the magnetic coils are not raised to temperatures above 400°C, where the isolation used between coil wraps could degrade and lead to electrical shorts. A water cooled cathode backplate is shown in figure 2, and is mounted to the test assembly as shown, but due to a leak in the water flow path could not be cooled during testing.

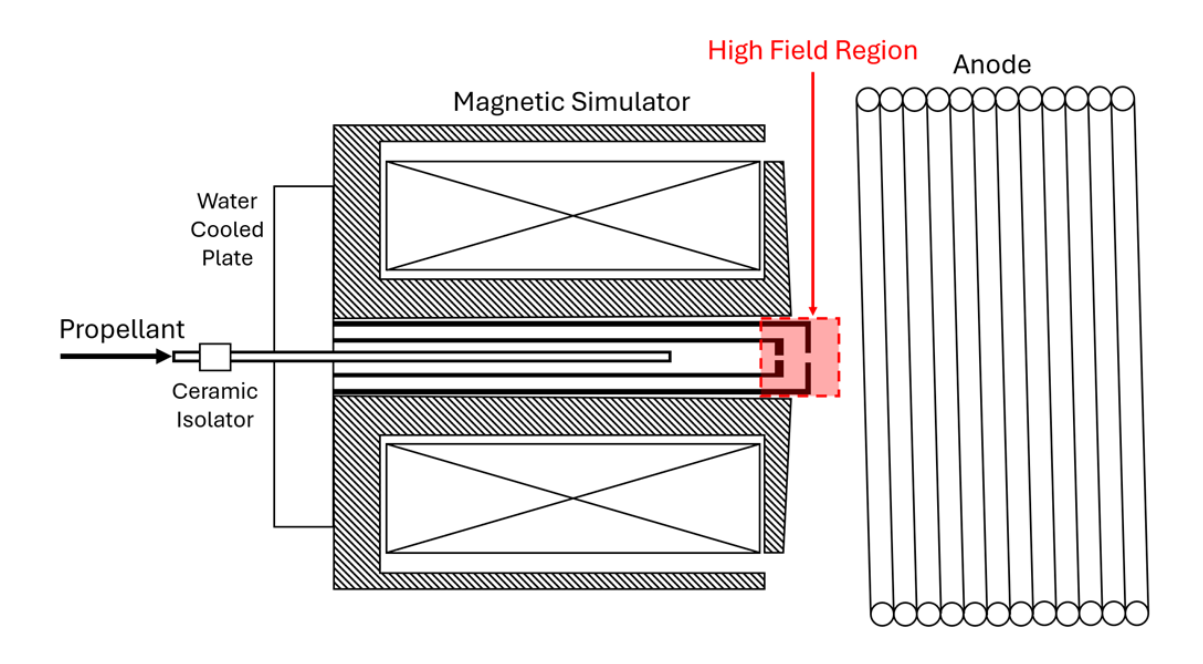


Figure 2. Cathode, Magnetic Simulator, and Anode Setup

#### B. Cathode Construction

The cathode assembly, presented in figure 3, is formed of three primary components - the keeper, cathode, and heater, each of which is electrically isolated from the other two by 6mm alumina silicate plates. The keeper and it's backplate are made of a single piece of machined graphite, with the orifice plate affixed using a high-temperature graphite adhesive. The keeper's outer diameter (OD) is 3.8cm, with 3.8mm thick walls; the orifice plate is the same thickness, with a 1.9cm orifice. Originally, a 1.3cm orifice had been used, but this led to excessive heating of the keeper; all data presented uses the larger orifice. The cathode consists of a kovar backplate, tantalum support tube, and the insert. The 2.5cm OD, 0.5mm thick tantalum tube is laser welded to the backplate to provide mounting and electrical connection points. The insert is formed from tungsten powder; BaCO<sub>3</sub>, CaCO<sub>3</sub>, and Al<sub>2</sub>O<sub>3</sub> powders in a 5:3:2 ratio; and  $Sc_2O_3$  powder. The formation process is described in [5], and allows for the formation of the insert in the geometry shown in figure 3, where the cathode orifice is made as part of the insert. The insert walls, including the orifice plate, are 5.5mm thick, the whole insert is 6.4cm long, and the orifice diameter is 7.6mm. This provides for a total possible emission area of  $27cm^2$ , and a minimum current density at 600A of  $22.4A/cm^2$ , although the anticipated density is anticipated to be significantly higher due to the attachment length not spanning the full insert.

To start up the cathode, a heater is needed to bring the insert to thermionic emission temperatures, which are in the 1000°C range for the insert used. Cathodes have typically used a resistive heating coil around the insert, which takes considerable time to heat the cathode, and can be damaged at high-temperature cathode operating points. Alternatives to this approach have been used, including a design where the propellant feed tube radiates to the insert [7]. The cathode presented in this paper uses a different method - a secondary electron emitter integrated in the feed tube emitting an electron current to the primary insert, thereby heating it. This secondary insert is a 6.3mm diameter cylinder with machined flats to allow gas flow, and is capable of supplying up to 15A of electron current to the primary insert. This secondary cathode is ignited through biasing at 400V negative of the primary insert to initiate a Paschen discharge, which triggers a plasma discharge arc that rapidly heats the heater insert to thermionic emission temperatures. Throughout the testing presented in this paper, the heating current was 1A, which was sufficient to consistently start the primary insert within 2 minutes. This startup time may also be attributed to the cathode's downstream orifice face being a thermionic emitter, which allows easier plasma generation between the cathode and keeper during startup. In a typical barium oxide hollow cathode, a similar process is achieved by gradual barium coverage of this orifice plate face, which contributes to their longer startup time.



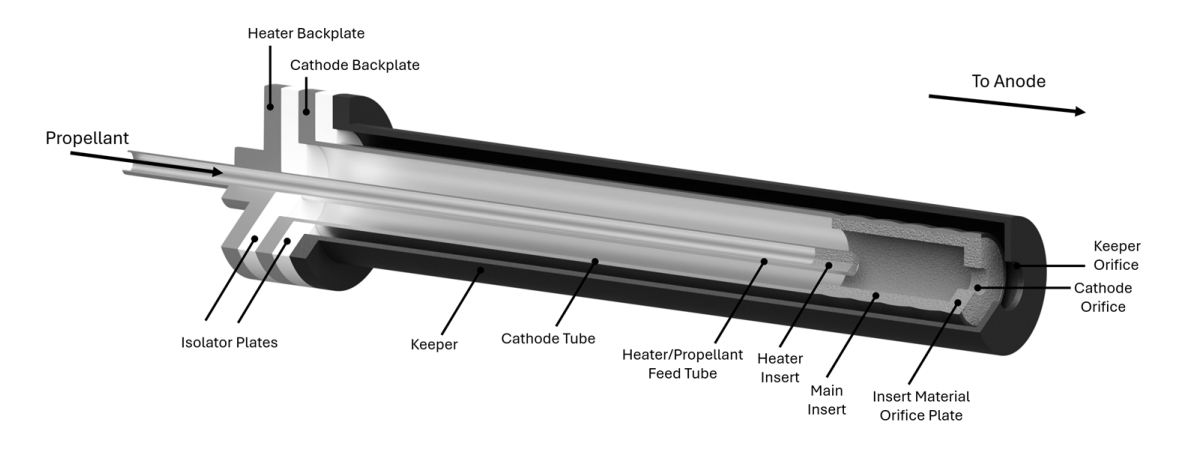


Figure 3. Render of the Cathode Assembly

## C. Electrical Setup

A simplified electrical diagram of the cathode, anode, keeper, and heater is shown in figure 4. This shows the keeper and anode biased positive of the cathode, and the heater biased negative of it. The anode power supply used is a set of 5 160V, 120A programmable DC power supplies operating in parallel to supply the full 600A of discharge current. The power supplies each have an upper limit of 5kW in power output, leading to an overall maximum power of 25kW, or 41.5V at 600A. Not shown in the diagram is the discharge filter used, which originally consisted of a inductor and capacitor network as described in [6]. The inductor was removed due to overheating at 400A and above, leaving just the 1mF capacitor network. Programmable DC power supplies are also used for the keeper (1000V, 20A) and heater (600V, 2.5A). Neither of these includes a filter as for the discharge, but both use the bypass and blocking diode power supply protection shown in [6]. Both the heater and keeper contain an in-line switch to prevent interference in voltage measurements from their respective supplies. The heater switch additionally prevents high current emission from the relatively small heater insert, which would damage the insert and heater power supply. Voltage measurements of each component are taken by sense leads separate from the power supply circuits, as shown in figure. For all leads but the heater, these use shielded coaxial cables to prevent electromagnetic interference in high-speed measurements. An additional sense lead is also connected to the magnetic simulator body to serve as an analog for a thruster body. The cathode-keeper voltage, anode current, and cathode-anode voltage are measured at high speed by an 8-bit, 8 GHz sample rate oscilloscope; the current is obtained from a 650A current transducer clamp.

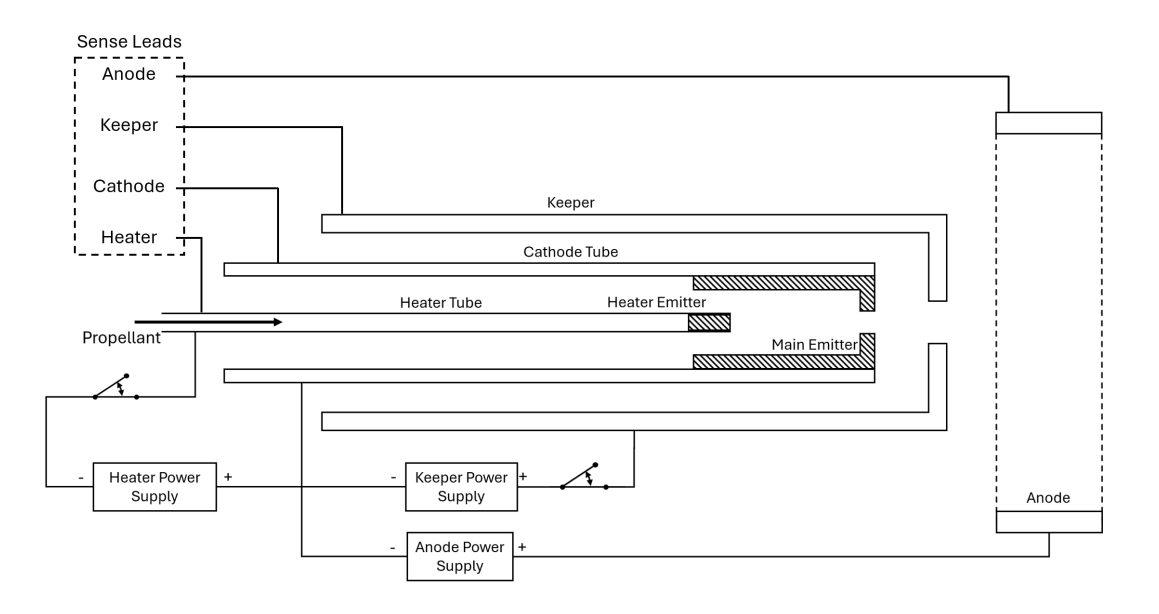


Figure 4. Electrical Setup Diagram

# III. Results

The cathode was successfully operated at currents ranging from 100A to 600A on both argon and krypton as propellant gasses, and at a variety of propellant flow rates on each gas. Distinct stable and unstable operation modes were observed on both propellants and at both low and high currents, with argon producing the unstable mode at more current-flow combinations than krypton. Low flow and high current operating points consistently produced this unstable mode, while high flow rates proportional to the current produced the stable mode. The cathode was run both with and without the magnetic field, where operating without the field produced a lower anode voltage by 10-15V and operation in the unstable mode persisting at higher flow rates. Data presented in this section was collected with the magnetic field active, as at the higher currents (>400A), stable operation could not be achieved without it.

Due to the need for temperature measurements without interference from the brightness of the plasma, the cathode was also operated at some times in a pulsed mode, where the anode supplies would periodically turn on and off at a given duty cycle. Re-ignition of the cathode in this mode was achieved solely using the anode voltage, and the full current was able to be re-established within a second of ignition. This was tested down to a duty cycle of 20% (2 seconds on, 8 seconds off), and continued to be successful over the  $\sim$ 2000 cycles tested.



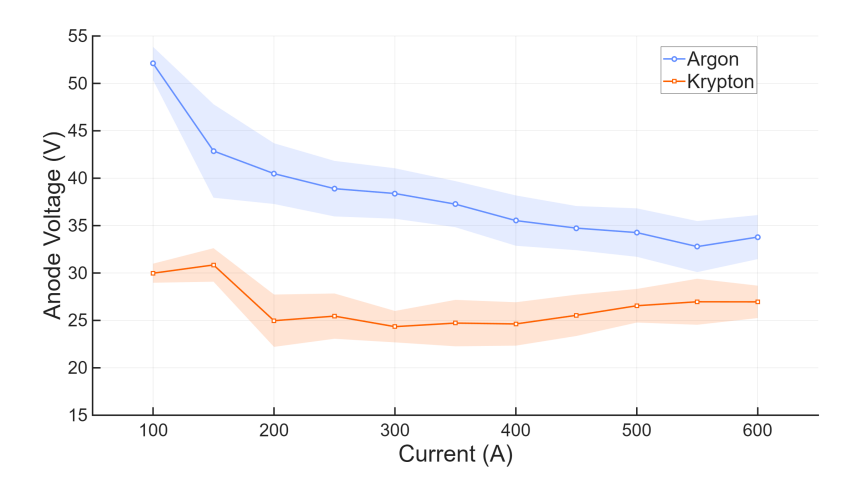


Figure 5. Current Sweeps at Flow Rate of 10% of Current in Amps Equivalent

Figure 5 presents discharge current sweeps on both argon and krypton with the flow rate fixed at 10% of the current when the flow is measured in amps equivalent, which is equivalent to 1.5sccm/A. This fraction was chosen to ensure stable operation modes on both gasses throughout the full current range, though notably krypton operated in the stable mode down to 5% at all currents. The shaded areas on the plot are two standard deviations above and below the time-averaged data, and so encompass roughly 96% of the recorded data points at the given operating condition. Operation on argon resulted in a distinct linear decrease in anode voltage as current increased from 200A to 600A, while the anode voltage on krypton had an increase with current, though at a much slower rate. Below 200A, the anode voltage rose sharply for both argon and krypton operation, which correlated with observed oscillations in the plasma brightness. This was initially suspected to be a hysteresis effect, as those currents were the first tested in each sweep, but a decreasing current sweep showed the same trend, indicating it was likely not. The brightness oscillations may indicate an ionization instability at these conditions, but further work on identifying this is outside the scope of this work, given the focus on high-current operation.

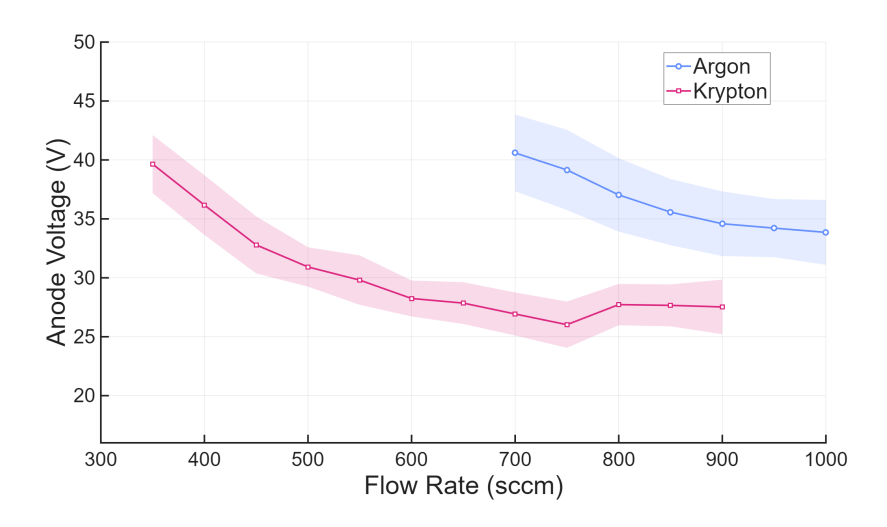


Figure 6. Flow Rate Sweeps at 600A Discharge Current

In figure 5, the current is varied proportionally to flow rate, figure 6 instead presents the anode voltages during flow rate sweeps at a fixed current of 600A. The shaded regions, as in figure 5, represent the two standard deviation range. The minimum flow tested on both propellants was set by the increasing discharge voltage causing the power requirement to exceed the 25kW maximum of the power supply network. This meant a minimum of 350sccm on krypton, and 700sccm on argon. As also seen in figure 5, operation on



argon produces consistently higher currents and wider voltage distributions. In both gasses, anode voltage tends to drop with increasing flow rate towards a plateau at the high flow rates. The krypton data shows a minium voltage at 750sccm, with a slight (2.5V) rise beyond it.

#### IV. Discussion

### A. Stable and Unstable Operation Modes

Cathodes tend to have two distinct operation modes - a high discharge voltage, unstable 'plume' mode, and a lower discharge voltage, stable 'spot' mode. Figure 7 shows the cathode operating in both a spot and plume mode. The plume mode is characterized by a diffuse plasma extending past the cathode, while the spot mode has a more concentrated, intense ball of plasma near the cathode orifice; these features are clearly identified in figure 7. As noted in the results section, the unstable mode was associated with lower flow rates and higher currents, which is expected for a plume mode [3, 9].

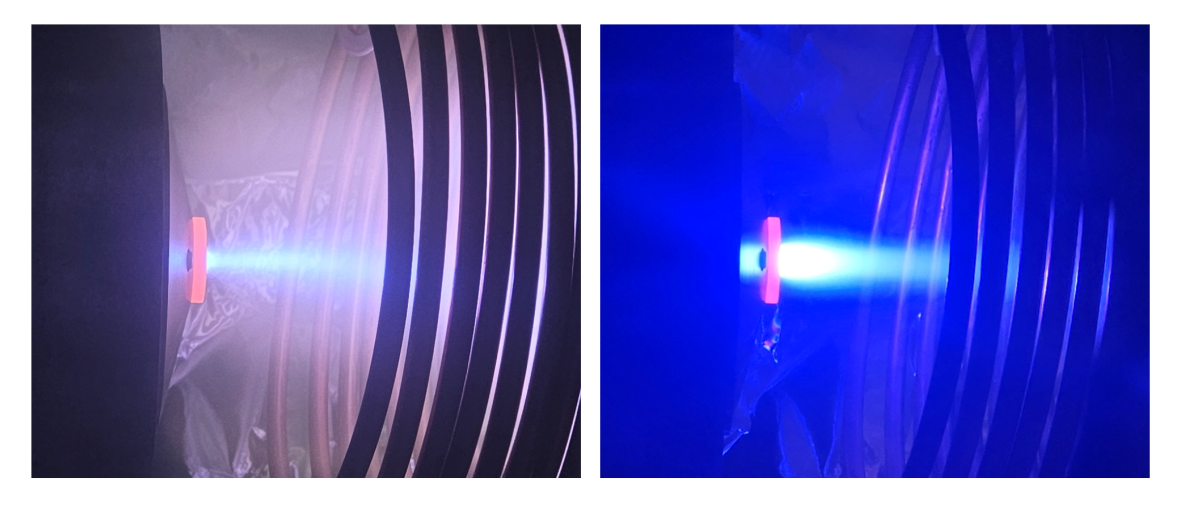


Figure 7. Cathode Operating in Plume (left) and Spot (right) Modes

Instabilities in the cathode's operation are associated with an increase in high-energy electrons within the plasma, which are damaging to the keeper [10] and cathode insert [11], and can severely limit the cathode lifetime. Figure 8 shows the ion energy distribution functions (IEDFs) for the plasma at the RPA's position. The three traces are all taken at 500A of discharge with decreasing flow rates of Argon. At the maximum flow rate, 1000 sccm, a single sharp peak exists at 12eV, with a small tail of highly energetic ions beyond that, but effectively none above 35eV. At the lower flow rates, the location of the peak remains the same, but the magnitude and length of the high energy ion tail increases significantly. The high and low flow operating points corresponded with the plasma appearing in a spot in plume mode respectively, similar to the images in figure 7, indicating that operating in the plume mode causes degradation to the cathode and anode. A similar set of traces was attempted on krypton as the propellant, but the RPA used was not able to reject electrons sufficiently to form clear and accurate distribution functions.

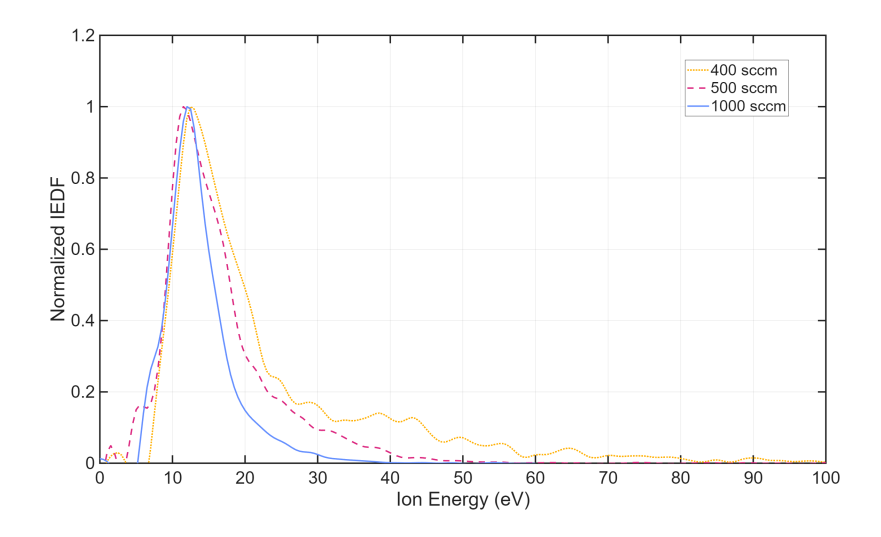


Figure 8. RPA Trace at Various Flow Rates of Argon at 500A Discharge Current

Using the oscilloscope, frequency data of the discharge voltage and current, along with the keeper voltage was acquired. Originally, the keeper voltage was planned to be used in identifying the operation modes, and determining the frequencies associated with the observed instabilities as in [1]. Due to low keeper voltages, however, the low measurement resolution from the oscilloscope made the data unusable. Instead, the discharge current has been used which, as shown in figure 9, shows distinct patterns for the two operating modes. Figure 9 is a Welch power spectrum density of the current signal at two operating points - one at lower flow and higher current to represent plume mode, and the other at high flow and low current to represent spot mode. The two curves are similar apart from a significantly higher power in the 150-1000kHz range oscillations for the plume mode, with large peaks at 150kHz and 300kHz as well as a smaller one at 700kHz. As all these instabilities lie above 100kHz, they are unlikely to be ionization or rotating magnetohydrodynamic instabilities [1, 12, 13]. Instead, it is likely these arise from ion acoustic turbulence (IAT) [10]; this would explain the strong dependence on flow rate, as increased neutral pressures within and near the cathode damp such oscillations through increased ion-neutral collisions [10]. The increased anode voltage with reducing flow may also be attributed to the onset of IAT, due to its increase in non-classical resistivity.

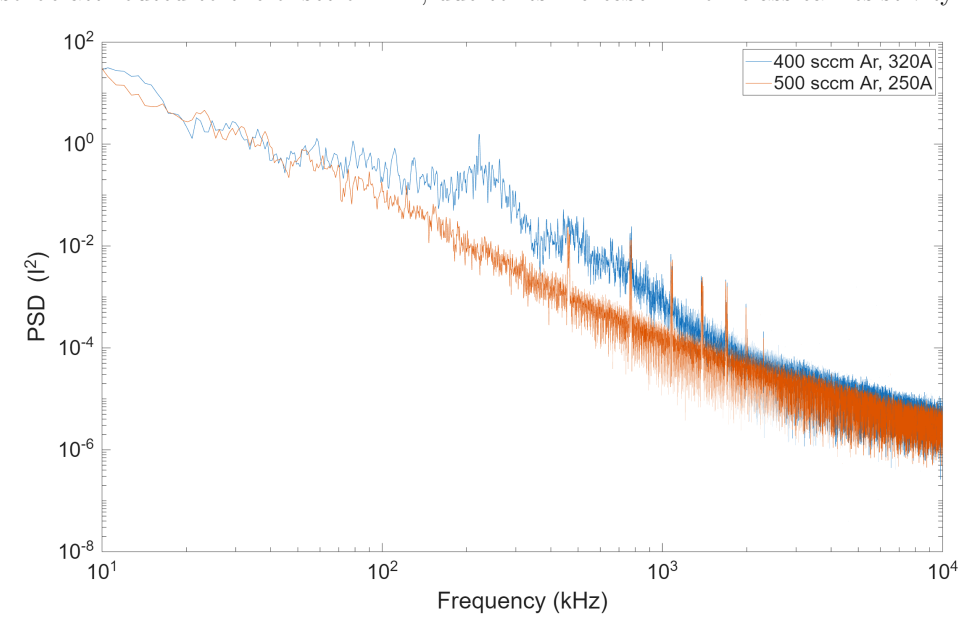


Figure 9. Welch PSD of Discharge Current at a Spot and Plume Mode on Argon



#### B. Lifetime Estimation

The cathode has been operated at currents of 300A or higher for a total of 20 hours during this testing campaign with no sign of degradation in performance. Flight cathodes, however, require lifetimes in the range of thousands of hours. The cathode was unable to be operated at high (>400A) currents for more than around 3 hours due to overheating of the magnetic coils and high-current vacuum feedthroughs, and overloading of the cryopump. As such, a preliminary estimate of the cathode's lifetime is presented.

Figure 10 shows a ternary phase diagram of Barium-Calcium-Aluminate at 1250°C, adapted from [13] for higher resolution, and to remove phases in the non-relevant high-Al<sub>2</sub>O<sub>3</sub> region. Note also that tie lines have been removed in some regions that are crucial to other BCA compositions such as 4:1:1, but are not for 5:3:2. Shown on the ternary plot are two compositions of BCA - 5:3:2 and 2:3:2, with the former being the initial composition and the latter representing an end-of-life composition as barium is lost from the cathode, and the loss rate of Al<sub>2</sub>O<sub>3</sub> and CaO are negligible in comparison. The equilibrium vapor pressure for both Ba and BaO established by the cermet is determined using the methods established in [15]. Throughout the projected lifetime of the cathode, the composition exists in two distinct 3-phase regions, the first containing a mixture of Ba<sub>4</sub>Al<sub>2</sub>O<sub>7</sub> (B4A), Ba<sub>3</sub>Al<sub>2</sub>O<sub>6</sub> (B3A), and pure CaO, then the second containing B3A, BaAl<sub>2</sub>O<sub>4</sub> (BA) and CaO. Both the B4A and B3A phases are solid solutions at their respective maximum solubility limits of CaO - 23% and 18%. As described in [15], the mixture stabilizes the phases, and thus reduces the BaO vapor pressure associated with the thermal decomposition of these phases.

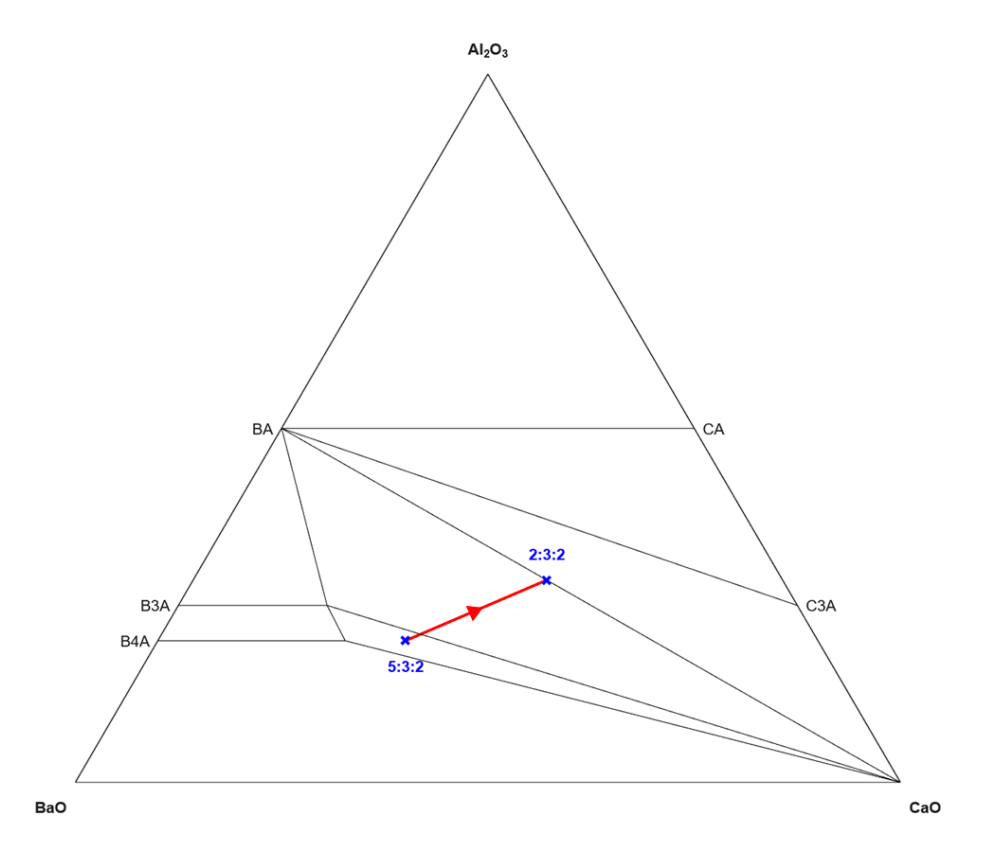


Figure 10. Predicted Change in 532 BCA Composition Over Operation Time

A study on the pore structure and internal barium migration mechanisms using the cermet inserts used for this cathode has not been conducted to this point, so an in-depth approach using the depletion depth over time such as in [11] can not be used. Instead a worst-case-scenario approach is used where the insert is assumed to always establish the equilibrium vapor pressure of the current cermet composition. This results in a linear dependence of barium content in time similar to [15], as opposed to the square root relationship presented in [11]. The loss of barium is taken as equal to the fraction of barium vapor to propellant gas multiplied by the rate of propellant molecules exiting through the cathode orifice. To determine the barium



gas fraction, the propellant pressure inside the cathode is calculated using the method described in [3], then the pressure ratio between the two gasses is equal to the mole fraction, as they are assumed to be ideal gasses in thermal equilibrium. Figure 11 shows profiles for barium loss from the insert over time at different temperatures up to 1000 hours. The barium mass used - 15.6 grams - is the overall mass of barium within the cathode insert at the time of manufacture. The curves for 1300°C and 1400 °C show a distinct change in slope when the barium mass drops below 14.2 grams, and extending the other two curves sufficiently would show the same result. This change in slope corresponds to the BCA composition crossing the B3A-CaO line and B3A becoming the new active phase as B4A is no longer present. As B3A imposes a lower BaO vapor pressure, the loss rate of barium is reduced as shown in the curves.

Ion bombardment can be safely neglected as a wear mechanism for the cathode, as the cathode temperatures exceed 900 °C and ion energies are below 15eV as shown in figure 8 for the high flow, stable case. These parameters mean that the barium thermal evaporation rate well exceeds the loss rate via ion bombardment [11].

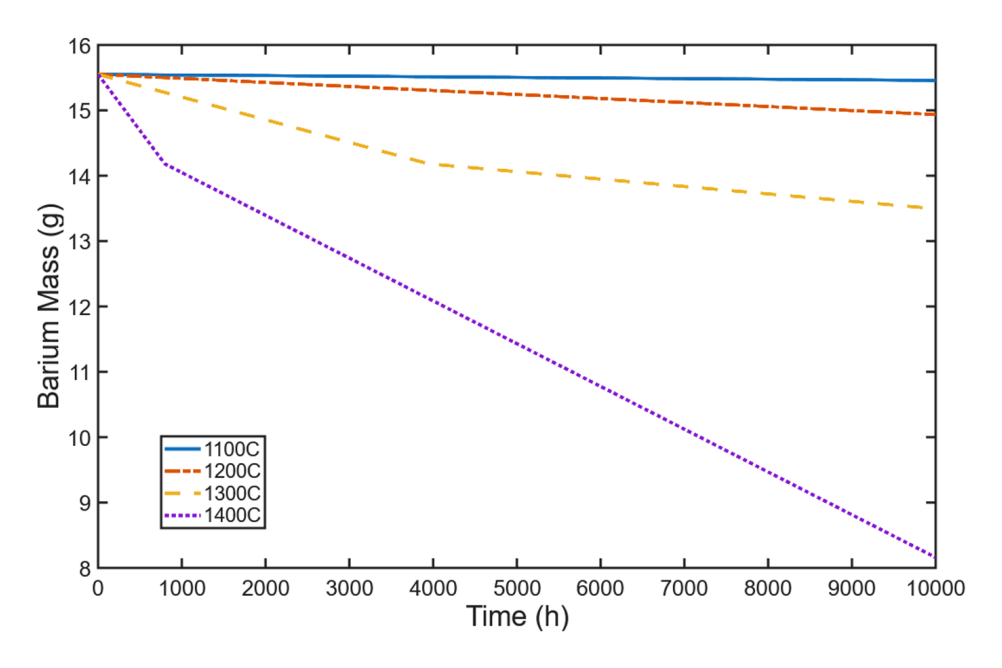


Figure 11. Barium Loss Profiles at Different Temperatures

Figure 12 shows the temperatures recorded at the cathode orifice face with the optical pyrometer for the full range of currents on both argon and krypton. The flow rates used at each condition are the same as in figure 5. The rest of the insert is likely to decrease in temperature moving upstream by up to 10-15% [11], but this measurement serves as a worst case. The temperatures are relatively linear with current, and no clear difference is observed between the two gasses.

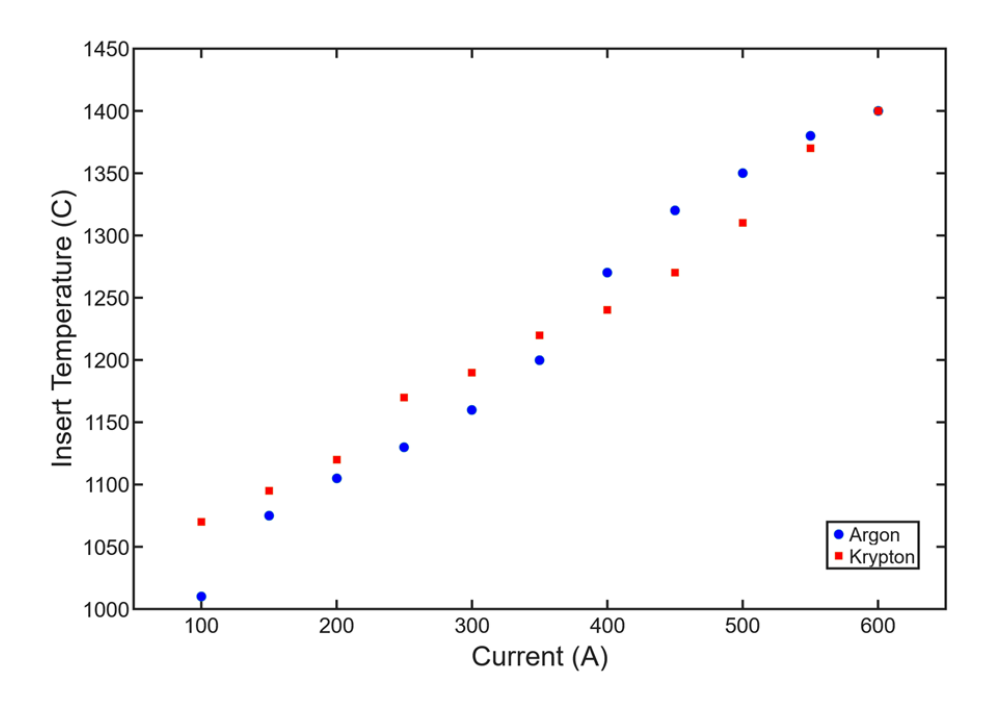


Figure 12. Optical Pyrometer Temperature Measurements of Cathode Orifice Plate

The time taken for the first phase transition - the aforementioned loss of the B4A phase, is plotted against the cathode operating currents, where the temperatures at each operating point in figure 12 are used in the vapor pressure calculations. The relationship is logarithmic, which follows from the linear current-time relationship, linear barium loss profile over time, and exponential relationship between temperature and vapor pressure. In the highest current operation mode, this first transition is predicted at 700 hours of operation. At this point, the drop in vapor pressure is likely to reduce the barium coverage rate of the tungsten surface, worsening the insert work function and thus increasing operation temperatures. This process may have been the observed persistent worsening in cathode performance (10% increase of the discharge voltage) between tests in [4]. The cathode is likely to continue operating beyond this point, and extending the plot indicates it may do so for an additional 10,000 hours 600A if the operating temperature is not changed significantly after the transition. Beyond this point, the 2:3:2 composition in figure 10 is reached, the B3A phase is lost, and Ba and BaO vapor pressures drop to negligibly small numbers, meaning the work function enhancement from barium coverage is no longer possible, and the cathode has reached a definite end-of-life.

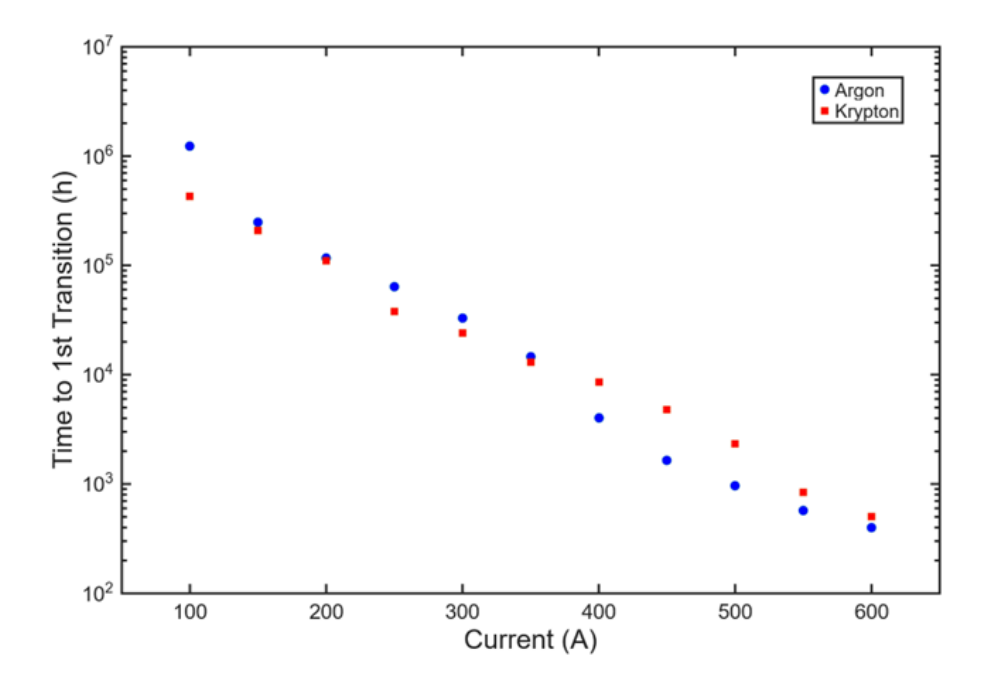


Figure 13. Time Until Barium Loss Causes a Change in the Phases Present in the BCA

#### C. Work Function Estimation

Based on the work in [16], the emission length of the insert can be estimated from the product of the orifice diameter and the insert pressure (calculated using the equation provided in [3]). From this, the insert's active emission area can be calculated, and with the insert temperature shown in figure 12, the Richardson-Dushman Equation can be used to estimate the insert's work function. Figure 14 shows this estimation for the 10% flow fraction operating condition over the full range of currents. For both propellants, the work function remains constant at 1.5eV below 300A, then begins to rise beyond that, to 1.7eV at the 600A operating condition. The presented values are the effective work function, which includes Schottky enhancement, and thus are reduced from the true material work function by the internal plasma's electric field at the emission surface. The trend potentially indicates the barium evaporation rate outpacing the supply rate through the pores of the material, as suggested by [2], however it is significantly less pronounced than expected. The observed rise may also be attributed to a change in emission area at these high current, but measurements of the internal plasma properties are required to fully assess this possibility.

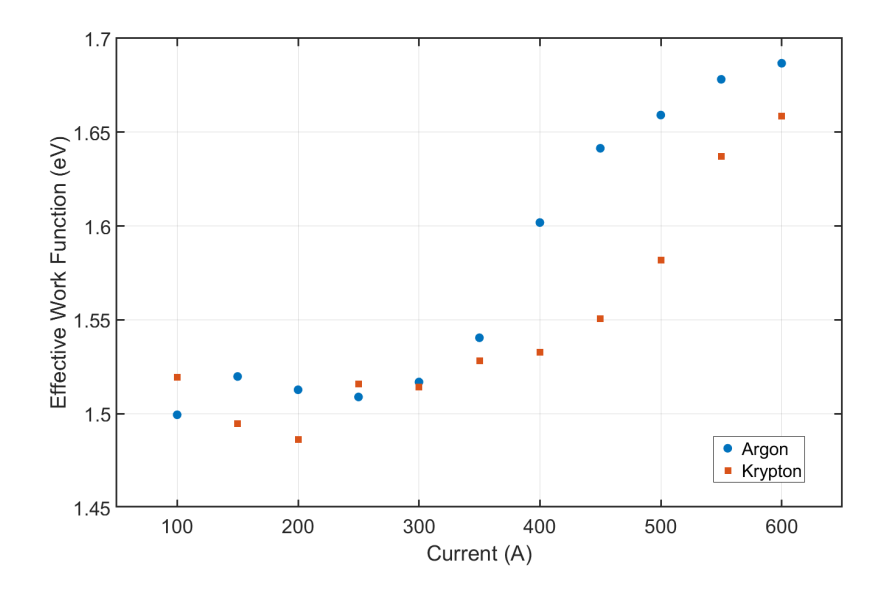


Figure 14. Estimated Insert Work Function

# V. Conclusion

This paper presents a 600A barium oxide based hollow cathode, with operation data on argon and krypton at various currents and flow rates. This characterization is conducted in a standalone cathode testing setup, with a magnetic coil simulating the field profile of a typical Hall Effect Thruster. Instabilities in the operation are identified and noted as likely caused by ion acoustic turbulence, which cause increased erosion of the cathode insert material and keeper, but are mitigated through maintaining a given current to flow rate ratio. From operating temperatures, and the chemistry of the insert, a preliminary lifetime model has been developed, which indicates that under worst-case approximations assuming barium depletion-limited life, the cathode is expected to have a lifetime of 10,000 hours. For an more comprehensive life study of the cathode, the material would have to be analyzed for the depletion depth of the BCA and its composition change over operation time. This would need to coincide with an investigation into the mechanism for supplying barium internal to the insert material to its surface as the cathode operates and how it compares to the rate of barium loss. At present, planned future work includes using a rapid motion stage to obtain plasma property profile and insert temperature profile along the inside of the cathode, followed by destructive imaging of a cathode operated at an extreme current density to create an accelerated life test.

# Acknowledgments

Martelli, R. would like to thank Alex Tutino, Tim Roberts, Rori Pumphrey, and Aaron Sawyer for their support in machining cathode and testing apparatus parts as well as preparing the vacuum testing facility for currents substantially beyond what has been previously achieved at CEPPE. This work was partially supported by NASA through the Joint Advanced Propulsion Institute (JANUS).



# References

- [1] Becatti, G., and Goebel, D. M., "500-A LaB6 Hollow Cathode for High Power Electric Thrusters," Vacuum, Vol. 198, 2022, p. 110895. https://doi.org/10.1016/j.vacuum.2022.110895
- [2] Goebel, D. M., Watkins, R. M., and Jameson, K. K., "LaB6 Hollow Cathodes for Ion and Hall Thrusters," Journal of Propulsion and Power, 2012. https://doi.org/10.2514/1.25475
- [3] Goebel, D. M., Katz, I., and Mikellides, I. G., "Fundamentals of Electric Propulsion," John Wiley & Sons, 2023.
- [4] Mantenieks, M., and Myers, R., "Preliminary Test Results of a Hollow Cathode MPD Thruster," 1991. https://api.semanticscholar.org/CorpusID:109227289
- [5] Farnell, C., Farnell, C., Williams, J. D., Williams, D., Nguyen, B. G., Greiner, K. E., and Ham, R. K., "Simplified Formation Process of a Low Work Function Insert," U.S. Patent 10,002,738, 2018.
- [6] Mooney, M. M., Thompson, S., Williams, J. D., Hall, S. J., Lev, D., Potrivitu, G., Becatti, G., and Ohlinger, W., "Recommended Practices in Electric Propulsion for Standalone Hollow Cathode Testing," presented at the 39th International Electric Propulsion Conference, Imperial College London, London, United Kingdom, 2025.
- [7] Goebel, D. M., and Payman, A. R., "Heaterless 300A Lanthanum Hexaboride Hollow Cathode," Review of Scientific Instruments, Vol. 94, No. 3, 2023, p. 033506. https://doi.org/10.1063/5.0135272
- [8] Goebel, Dan M.; Watkins, Ron M., 2005, "High current hollow cathodes for high power ion and hall thrusters", https://hdl.handle.net/2014/37801, 2005 AIAA Joint Propulsion Conference, Tuscon, Arizona, July 10-13, 2005, JPL Open Repository
- [9] Sakai, S. Katayama, T., Aoyagi, J., Takegahara, H., "Discharge Modes and Characteristics of Hollow Cathode," Presented at the 30th International Electric Propulsion Conference, Florence, Italy, https://electricrocket.org/IEPC/IEPC-2007-215.pdf
- [10] Jorns, B. A., Mikellides, I. G., Goebel, D. M., and Ortega, A. L. "Mitigation of Energetic Ions and Keeper Erosion in a High-Current Hollow Cathode", IEPC-2015-134, 34th IEPC, Hyogo-Kobe, Japan, July 2015
- [11] Goebel, D., "Extending Hollow Cathode Life for Electric Propulsion for Long-Term Missions," presented at the Space 2004 Conference and Exhibit, San Diego, California, 2004. https://doi.org/10.2514/6.2004-5911
- [12] Becatti, G., and Goebel, D. M. "Observation of Rotating Magnetohydrodynamic Modes in the Plume of a High-Current Hollow Cathode," Journal of Applied Physics, Vol. 129, 2021, 033304. doi:10.1063/5.0028566.
- [13] Dodson, C. A., Perez-Grande, D., Jorns, B. A., Goebel, D. M., and Wirz, R. E. "Ion Heating Measurements on the Centerline of a High-Current Hollow Cathode Plume," Journal of Propulsion and Power, Vol. 34, No. 5, 2018, pp. 1225–1234. Doi:10.2514/1.B36788.
- [14] Wolten, G. M., "An Appraisal of the Ternary System BaO-CaO-Al2O3.," 1980. https://apps.dtic.mil/sti/html/tr/ADA091684/
- [15] Lipeles, R. A., and Kan, H. K. A., "Chemical Stability of Barium Calcium Aluminate Dispenser Cathode Impregnants," Applications of Surface Science, Vol. 16, No. 1, 1983, pp. 189–206. https://doi.org/10.1016/0378-5963(83)90067-3
- [16] Wordingham, C. J., Taunay, P-Y. C. R., Choueiri, E. Y., "The attachment length in orificed hollow cathodes," Plasma Sources Science and Technology Vol. 31, No. 1, 2022. https://doi.org/10.1088/1361-6595/ac3d3f.

